Assessment of the induced seismicity potential in pressurized and depleted reservoirs: the role of fault permeability

Haiqing Wu[1),2),*], Victor Vilarrasa[2),3),4)], Silvia De Simone[5)], Maarten Saaltink[1),2)] and Francesco Parisio[6)]

1) Department of Civil and Environmental Engineering (DECA), Universitat Politécnica de Catalunya (UPC), Jordi Girona 1-3, 08034 Barcelona, Spain
2) Associated Unit: Hydrogeology Group (UPC-CSIC)
3) Institute of Environmental Assessment and Water Research (IDAEA), CSIC, c/ Jordi Girona 18, 08034 Barcelona, Spain
4) Mediterranean Institute for Advanced Studies (IMEDEA), Spanish National Research Council (CSIC), Esporles, Spain
5) Univ Rennes, CNRS, Géosciences Rennes - UMR 6118, Rennes, France
6) Chair of Soil Mechanics and Foundation Engineering, Technische Universität Bergakademie Freiberg, Germany
*Corresponding author: haiqing.wu@upc.edu

1. Introduction

Induced seismicity during reservoir pressurization or depletion has become a widespread issue (Ferronato et al., 2010; Ellsworth 2013) as a result of the proliferation of geo-energy projects (Foulger et al., 2018). Faults intersecting the injection/pumping formation undergo pore pressure and stress changes, affecting their stability. The hydraulic properties of faults (e.g., permeability) control the pore pressure change which, through poromechanical effects, increases the total stress in the rock. Faults cause additional stress change (Gheibi et al., 2017) that is further enhanced by fault offset (Buijze et al., 2017), which can increase the frequency of induced earthquakes. Thus, predicting the stress variation in presence of displaced faults is particularly relevant in order to minimize the induced seismicity risk.
Analytical solutions provide accurate and fast predictions and are well suited to gain insights into the physical mechanisms. For the problem of reservoir pressurization/depletion, Eshelby's inclusion theory (Eshelby, 1957) is at the heart of several existing analytical solutions that either assume non-displaced faults (e.g., Segall, 1992; Soltanzadeh and Hawkees, 2008; Wang et al. 2016) or displaced but permeable faults (Jansen et al., 2019). Since no solution existed for low-permeable faults that cross the reservoir with an offset, we have developed one (Wu et al., 2020). In this paper, we analyse the difference in terms of induced seismicity potential in response to injection/pumping into a reservoir crossed by a displaced fault that could be either permeable or impermeable.

2. Methods

We compute the stress changes arising in a deep reservoir crossed by a displaced fault (considered in the limiting cases of being either fully permeable or impermeable) as a result of fluid injection or production through the inclusion theory (Eshelby, 1957; Rudnicki, 2011). The stress variation σ_{ij} in the reservoir as a result of pore pressure changes is (Wu et al., 2020)

$$\sigma_{ij}(x,y) = \frac{(1-2\nu)\alpha\Delta p}{2\pi(1-\nu)}\left[G_{ij}(x,y) - \pi\delta_{ij}\delta_{\Omega}\right], \quad (1)$$

where Ω is the inclusion domain, G_{ij} represents the surface integral of Green's function for stress, x and y are the Cartesian coordinates, α is the Biot's coefficient, ν is the Poisson's ratio, Δp is the pore pressure change, δ_{ij} is the Kronecker delta, and δ_{Ω} is the modified Kronecker delta, which equals 1 if $(x,y) \in \Omega$ or 0 if $(x,y) \notin \Omega$. We adopt the sign convention that negative stress denotes compression and a negative pore pressure change refers to depletion.
The difference between permeable and impermeable faults is the surface integral G_{ij}. While for the former case, pore pressure changes on both sides of the fault within the reservoir, it only changes on the side of the fault where injection or depletion takes place for the latter case. After

solving the induced stress, we apply the mobilized friction coefficient μ_{mob} to assess fault stability

$$\mu_{\mathrm{mob}} = \left|\tau + \tau^0\right| \Big/ [-(\sigma_{\mathrm{n}}^{'} + \sigma_{\mathrm{n}}^{'0})], \tag{2}$$

where σ_{n} and τ are the induced normal and tangential stress components on the fault plane, respectively, superscript 0 represents the initial state and the normal stress with a superscript ' means the effective normal stress. Thus, the fault is stable for $\mu_{\mathrm{mob}} < \mu_{\mathrm{st}}$, critical for $\mu_{\mathrm{mob}} = \mu_{\mathrm{st}}$, while unstable for $\mu_{\mathrm{mob}} > \mu_{\mathrm{st}}$, in which μ_{st} is the static friction coefficient. The initial mobilized friction coefficient μ_{mob}^0 to can be calculated using Eq. (2). μ_{mob}^0 only depends on the initial stress state and the fault dip.

The dimensionless maximum fault slip size S_{Dmax} is adopted to quantitatively evaluate the fault slip potential, and thus, the induced seismicity potential

$$S_{\mathrm{Dmax}} = \max(\ell_i)/h, \tag{3}$$

where ℓ_i is a continuous interval in coordinate y with $\mu_{\mathrm{mob}} > \mu_{\mathrm{st}}$ (the unstable patch), which is normalized by the reservoir thickness h. We assume $S_{\mathrm{Dmax}} = 0.01$ as the threshold for fault slip. We consider a base case scenario for a pressurized reservoir whose properties are derived from laboratory measurements on Berea sandstone (Makhnenko et al., 2015; Wu et al., 2020) (Table 1). We perform a parametric space analyses to explore the effects of the initial stress state and pore pressure changes on the stress variation and the induced seismicity potential. We compare the results for the two cases of permeable and impermeable faults with fluid injection into the hanging wall of the fault to understand the influence of the hydraulic properties of faults.

Table 1: Properties of Berea sandstone and the initial stress state of the reservoir

Parameter	Physical meaning	Value	Unit
θ	Fault dip	60	°
h	Reservoir thickness	300	m
E	Young's modulus	11.87	GPa
ν	Poisson's ratio	0.29	-
α	Biot's coefficient	0.7	-
Δp	pressure buildup	20	MPa
p^0	Initial pore pressure	35	MPa
σ_{yy}^0	Initial vertical stress	-70	MPa
k_0	Stress ratio of horizontal to vertical stress	0.6	-
μ_{st}	Static friction coefficient	0.6	-

3. Results and Discussion

We evaluate the induced shear and normal stress components on the fault plane for a permeable (Fig. 1a and 1b) and an impermeable fault (Fig.1c and 1d). For the permeable fault, the induced stress is symmetrical with respect to $y = 0$. The corner points that arise due to fault offset are singular, such that the induced shear stress tends to infinity. The induced normal stress has a reverse behavior with respect to the induced shear stress (compare Fig. 1a and 1b). The entire fault plane, except for a small vicinity at the corners P2 and P3, shows a negative induced normal stress, which implies an increase in slip resistance, i.e., the destabilizing effect of pore pressure within the reservoir is compensated by an increase in the total normal stress.

Unlike the permeable case, the induced shear and normal stress components are not symmetrical with respect to $y = 0$ for the impermeable fault, but the feature of reverse behavior for shear and normal stress components still holds (compare Fig. 1c and 1d). The induced shear and normal stress components also tend to infinity at the corners of the pressurized reservoir as

a consequence of injecting on the left-hand side of the fault. These stress singularities in both the permeable and impermeable faults are unrealistic for faults in nature because they are not produced by the physical properties of faults but by the integration of the Green's function.

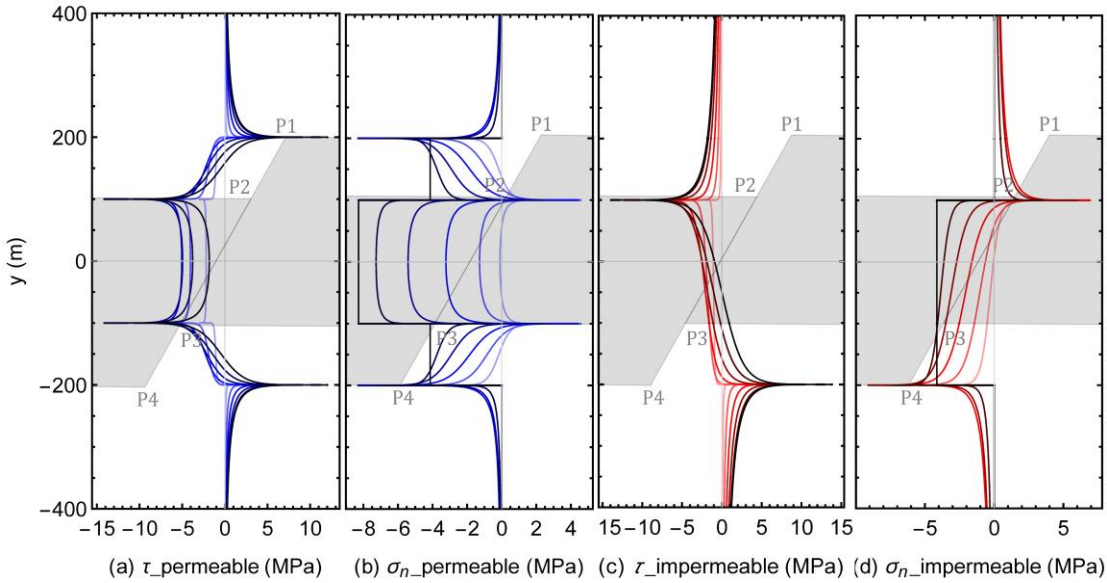

Figure 1: Comparison of the induced (a) shear stress and (b) normal stress for a permeable fault, and (c) shear stress and (d) normal stress for an impermeable fault on the fault plane for different dips and a fault offset of 100 m. The color lines range from light to dark, indicating the dip angle, which changes from 15° to 90° with an increment of 15°. A schematic of the reservoir geometry, with the four corners, is indicated by the grey background.

We explore the influence of the initial stress state by applying different values of the initial mobilized friction coefficient because μ_{mob}^{0} monotonically increases with the initial deviatoric stress under a given fault dip, and of the operational aspects by applying different pressure build-up as Δp strongly depends on the injected volume and injection rate (Wu et al., 2018). The dimensionless maximum fault slip size S_{Dmax} increases with μ_{mob}^{0} and Δp_{D} for both permeable and impermeable faults (Fig. 2), which indicates that (1) the larger the initial deviatoric stress, the more critical the fault; (2) a larger pressure build-up is more likely to induce seismicity and thus the maximum sustainable injection pressure (Rutqvist et al., 2007) should be calculated to minimize the risk of inducing seismicity.

For a given pressure build-up, the rate of increase in S_{Dmax} with increasing μ_{mob}^{0} is not steady and is controlled by the failure process of the formation (Fig. 2). The fault is stable while μ_{mob}^{0} is smaller than its critical value, which corresponds to the threshold for fault slip (here assumed as $S_{\mathrm{Dmax}} = 0.01$). Once μ_{mob}^{0} is larger than its critical value, the fault will slip and S_{Dmax} increases up to $S_{\mathrm{Dmax}} \approx 0.25$. Then, for a certain interval in μ_{mob}^{0}, the increasing rate in S_{Dmax} decreases, and finally such rate sharply increases (Fig. 2). These three phases of the increasing rate in S_{Dmax} correspond to the progressive failure of the pressurized reservoir, the initiation of failure in the caprock or bedrock and the asymptotic failure of the caprock or bedrock, respectively. The critical value of μ_{mob}^{0} linearly decreases with increasing Δp_{D}. Similarly, for a given initial mobilized friction coefficient, the fault always remains stable when Δp_{D} is lower than its critical value, which also corresponds to $S_{\mathrm{Dmax}} = 0.01$ in this case. The fault begins to slip when Δp_{D} exceeds its critical value, and the increasing rate in S_{Dmax} with Δp_{D} is also similar to the case of increasing μ_{mob}^{0}, which is controlled by the identical failure process of the formation. The critical value of Δp_{D} also linearly decreases with the increase in μ_{mob}^{0} (Fig. 2).

Comparison between the permeable and impermeable cases shows that S_{Dmax} in the impermeable case is always larger than the one in the permeable case under any initial and injection conditions. Generally, the magnitude of S_{Dmax} for the former is 3 to 5 times greater than the one for the latter, and thus, the induced seismicity potential, for a given initial

mobilized friction coefficient and pressure build-up (or pressure depletion). Moreover, both the critical values of μ^0_{mob} and Δp_{D} are smaller for an impermeable fault than for a permeable one, which implies that the former would rupture at a lower μ^0_{mob}, i.e., less deviatoric stress, and at a smaller pressure buildup than the latter.

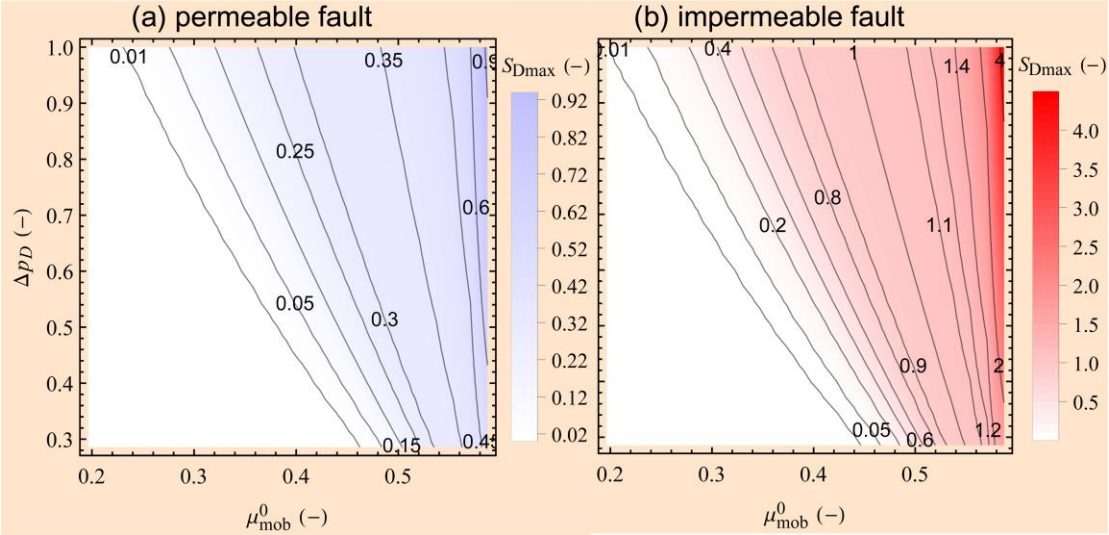

Figure 2: Dimensionless maximum fault slip size (S_{Dmax}) as a function of the initial mobilized friction coefficient μ^0_{mob} and the dimensionless pressure build-up Δp_{D} normalized by the initial pore pressure for (a) permeable and (b) impermeable faults. The numbers on the contours denote the values of S_{Dmax}. The maximum of μ^0_{mob} is limited by μ_{st} to ensure the fault is stable at the initial state.

4. Conclusions

We analyse the induced seismicity potential of permeable and impermeable faults as a result of reservoir pressurization using a recently developed analytical solution that is based on the inclusion theory. The induced seismicity potential of impermeable faults is always larger than that of permeable faults under any initial and injection conditions. The maximum size of the fault undergoing slip for the former is 3 to 5 times greater than that for the latter under a given initial mobilized friction coefficient and pressure build-up. An impermeable fault would rupture at a lower deviatoric stress, and at a smaller pressure build-up than a permeable one. Thus, geological sites with a lower initial deviatoric stress are intrinsically less prone to fluid injection-induced seismicity. This finding is useful for site selection in geo-energy projects. Our results support the pressure managing strategy of controlling the wellhead injection pressure below the maximum sustainable pressure.

Acknowledgements

H.W. would like to acknowledge the financial support received from the AGAUR (Generalitat de Catalunya) through the ‘‘grant for universities and research centers for the recruitment of new research personnel (FI-2019)’’. H.W. and V.V. acknowledge financial support from the “ZoDrEx” project, which has been subsidized through the ERANET Cofund GEOTHERMICA (Project no. 731117), from the European Commission and the Spanish Ministry of Economy, Industry and Competitiveness (MINECO) (PCI2018-093272). V.V. acknowledges funding from the European Research Council (ERC) under the European Union's Horizon 2020 Research and Innovation Programme through the Starting Grant GEoREST (www.georest.eu), grant agreement No. 801809. V.V. also acknowledges support by the Spanish Ministry of Science and Innovation (Project CEX2018-000794-S). F.P. acknowledges funding from the Deutsche Forschungsgemeinschaft (DFG, German Research Foundation) – project number PA

3451/1-1. S.D.S. acknowledges financial support from the SAD2018 project funded by the Brittany Region and from ANR LabCom Project eLabo ANR-17-LCV2-0012.

References

Buijze, L., van den Bogert, P. A., Wassing, B. B., Orlic, B., & ten Veen, J. (2017). Fault reactivation mechanisms and dynamic rupture modelling of depletion-induced seismic events in a Rotliegend gas reservoir. Netherlands Journal of Geosciences, 96(5), s131-s148.

Ellsworth, W. L. (2013). Injection-induced earthquakes. Science, 341(6142), 1225942.

Eshelby, J. D. (1957). The determination of the elastic field of an ellipsoidal inclusion and related problems. Proc. R. Soc. London, Ser. A, 241, 376-396. http://dx.doi.org/10.1098/rspa.1957.0133.

Ferronato, M., Gambolati, G., Janna, C., & Teatini, P. (2010). Geomechanical issues of anthropogenic CO_2 sequestration in exploited gas fields. Energy Conversion and Management, 51(10), 1918-1928.

Foulger, G. R., Wilson, M. P., Gluyas, J. G., Julian, B. R., & Davies, R. J. (2018). Global review of human-induced earthquakes. Earth-Science Reviews, 178, 438-514.

Gheibi, S., Holt, R. M., & Vilarrasa, V. (2017). Effect of faults on stress path evolution during reservoir pressurization. International Journal of Greenhouse Gas Control, 63, 412-430.

Grigoli, F., Cesca, S., Rinaldi, A. P., Manconi, A., López-Comino, J. A., Clinton, J. F., ... & Wiemer, S. (2018). The November 2017 Mw 5.5 Pohang earthquake: A possible case of induced seismicity in South Korea. Science, 360(6392), 1003-1006.

Jansen, J. D., Singhal, P., & Vossepoel, F. C. (2019). Insights from closed‐form expressions for injection‐and production‐induced stresses in displaced faults. Journal of Geophysical Research: Solid Earth. 124(7), 7193-7212.

Makhnenko, R. Y., & Labuz, J. F. (2015). Dilatant hardening of fluid‐saturated sandstone. Journal of Geophysical Research: Solid Earth, 120(2), 909-922.

Rudnicki, J. W. (2011). Eshelby's technique for analyzing inhomogeneities in geomechanics. In Mechanics of crustal rocks (pp. 43-72). Springer, Vienna.

Rutqvist, J., Birkholzer, J., Cappa, F., & Tsang, C. F. (2007). Estimating maximum sustainable injection pressure during geological sequestration of CO2 using coupled fluid flow and geomechanical fault-slip analysis. Energy Conversion & Management, 48(6), 1798-1807.

Segall, P. (1992). Induced stresses due to fluid extraction from axisymmetric reservoirs. Pure Appl. Geoph., 139 (3-4), 535-560. https://doi.org/10.1007/BF00879950.

Soltanzadeh, H., & Hawkes, C. (2008). Semi-analytical models for stress change and fault reactivation induced by reservoir production and injection. J. Petr. Sc. Eng., 60, 71-85. https://doi.org/10.1016/j.petrol.2007.05.006.

Wang, L., Bai, B., Li, X., Liu, M., Wu, H., & Hu, S. (2016). An analytical model for assessing stability of pre-existing faults in caprock caused by fluid injection and extraction in a reservoir. Rock Mechanics and Rock Engineering, 49(7), 2845-2863.

Wu, H., Bai, B., Li, X. (2018). An advanced analytical solution for pressure buildup during CO_2 injection into infinite saline aquifers: The role of compressibility. Advances in Water Resources, 112: 95-105. DOI: 10.1016/j.advwatres.2017.12.010

Wu, H., Vilarrasa, V., De Simone, S., Saaltink, M. & Parisio, F. (2020). Analytical solution to assess the induced seismicity potential of faults in pressurized and depleted reservoirs. Journal of Geophysical Research: Solid Earth. Under review.